BIOCHEMISTRY
including biophysical chemistry & molecular biology

ARTICLE

pubs.acs.org/biochemistry

The E2 Domains of APP and APLP1 Share a Conserved Mode of Dimerization

Sangwon Lee,[†] Yi Xue,[†] Jian Hu,[†] Yongcheng Wang,[†,§] Xuying Liu,[†] Borries Demeler,[‡] and Ya Ha[*,†]

[†]Department of Pharmacology, Yale School of Medicine, New Haven, Connecticut 06520, United States

[‡]Department of Biochemistry, University of Texas Health Science Center at San Antonio, San Antonio, Texas 78229, United States

Supporting Information

ABSTRACT: Amyloid precursor protein (APP) is genetically linked to Alzheimer's disease. APP is a type I membrane protein, and its oligomeric structure is potentially important because this property may play a role in its function or affect the processing of the precursor by the secretases to generate amyloid β-peptide. Several independent studies have shown that APP can form dimers in the cell, but how it dimerizes remains controversial. At least three regions of the precursor, including a centrally located and conserved domain called E2, have been proposed to contribute to dimerization. Here we report two new crystal structures of E2, one from APP and the other from APLP1, a mammalian APP homologue. Comparison with an earlier APP structure, which was determined in a different space group, shows that the E2 domains share a conserved and antiparallel mode of dimerization. Biophysical measurements in solution show that heparin binding induces E2 dimerization. The 2.1 Å resolution electron density map also reveals phosphate ions that are bound to the protein surface. Mutational analysis shows that protein residues interacting with the phosphate ions are also involved in heparin binding. The locations of two of these residues, Arg-369 and His-433, at the dimeric interface suggest a mechanism for heparin-induced protein dimerization.

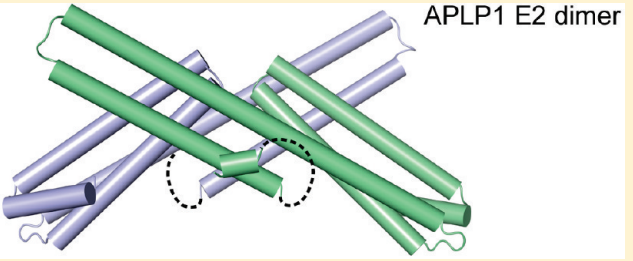

Amyloid precursor protein (APP) has generated great interest in both medical and basic research. Mutations in APP are known to cause familial Alzheimer's disease (for a recent review, see ref 1), yet the physiological function of the precursor protein remains elusive. In mammals, APP has two homologues, APLP1 and APLP2.[2,3] Knocking out all three genes is lethal to the animal.[4] APP and the two APLPs are type I membrane proteins[5] and are found both inside the cell and on the cell surface. Proteolysis by secretases releases various fragments of the protein from the membrane. These include amyloid β-peptide, widely believed to play an important role in Alzheimer's disease,[6] a number of different ectodomain fragments that have been shown to have various biological activities (e.g., see refs 7−9), and a small intracellular domain that is thought to function in transcriptive regulation (e.g., see refs 10−12).

The oligomeric structure of APP is potentially important because this may affect its proteolytic processing[13] or play a role in the transmembrane signaling mechanism in which the protein is involved.[14] Biochemical and cell biological studies have shown that APP can form dimers in the cell,[14−18] but many questions remain controversial. For example, which domain of the membrane protein is responsible for dimerization?[16,19,20] Is dimerization obligatory or induced by ligand binding (e.g., heparan sulfate proteoglycans[20,21])? The matter is further complicated by the possibilities that APP may heterodimerize with the APLPs and that dimerization can occur not only *in cis* but also *in trans* between molecules from different cells.[16,18]

The ectodomains of APP and APLPs have two conserved regions called E1 and E2 (Figure 1A), both of which have been proposed to contribute to dimerization. A recently determined crystal structure of E1 reveals an interesting dimeric arrangement of the protein in which the dimeric contact is mediated exclusively through the N-terminal portion of the molecule, a substructure called the growth factor-like domain (GFLD).[20] In an earlier study, however, the isolated GFLD crystallized as monomers.[22] The crystal structures of E2[19,23] and the NMR structure of a fragment of it[24] have also been determined. The crystal structure shows that E2 forms an antiparallel dimer.[19] Nevertheless, the hypothesis that E2 may function as the dimerization domain of the full-length molecule was recently challenged by the observation that the E2 domain of the *Caenorhabditis elegans* homologue APL-1 has been crystallized as monomers.[25] To help clarify the oligomeric structure of E2, here we report two new crystal structures of E2, one from APP and the other from APLP1, and show that they share the same mode of antiparallel dimerization. We also show for the first time that heparin binding induces E2 dimerization. Because members of the APP family of proteins travel to the cell surface and can be secreted into the extracellular matrix, the possibility that heparan

Received: November 18, 2010
Revised: May 4, 2011
Published: May 16, 2011

ACS Publications © 2011 American Chemical Society

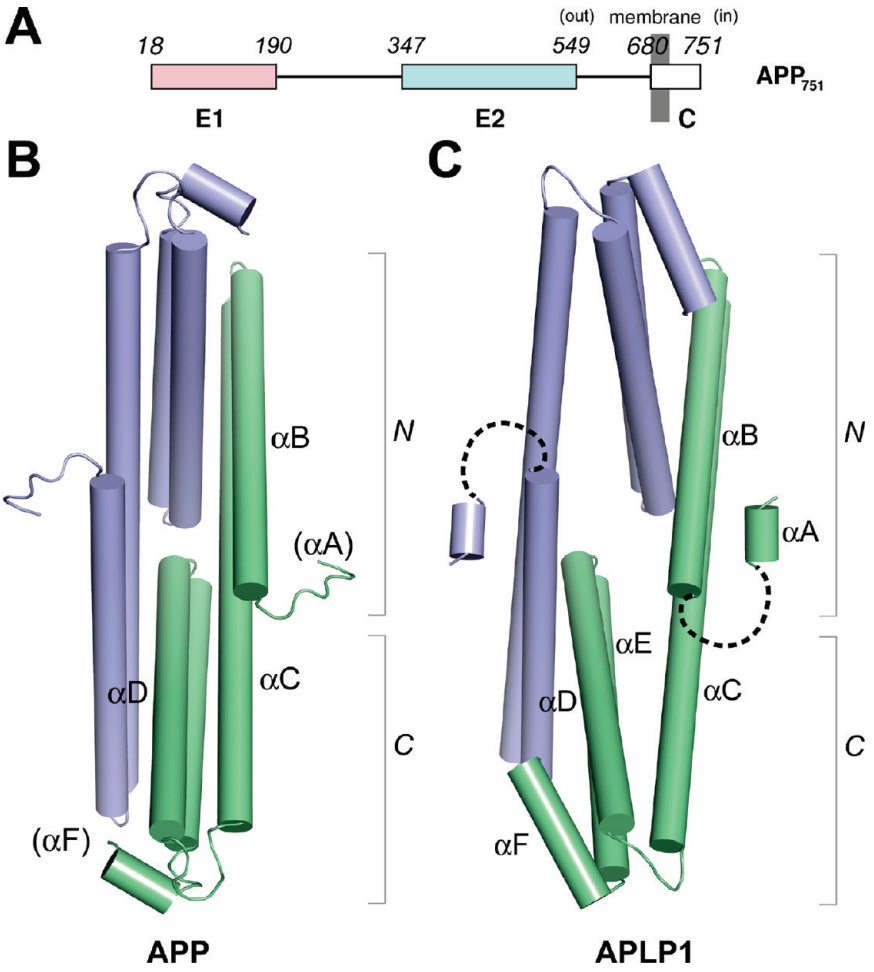

Figure 1. E2 domains of APP and APLP1 have similar dimeric structures. (A) Domain structure of APP. The residue numbers shown above the diagram are from the common APP isoform-751. (B) Structure of the E2 domain of APP in crystal form "B". Helix αA is disordered in the crystal lattice. The two protein protomers are shown in different colors. Helices are shown as cylinders. The two subdomains (N and C) are also labeled. (C) Structure of the E2 domain of APLP1. In the crystal, helix αA is domain-swapped. Shown here are the corresponding helices from neighboring molecules (the loop connecting αA to αB is represented by the dashed line). These illustrations and those in Figure 3C and Figure 5 were generated with PyMol.

sulfate proteoglycans might modulate their oligomerization states has important biological implications.

MATERIALS AND METHODS

Subcloning, Protein Expression, and Purification. The procedures for the expression and purification of native and Se-Met-substituted APP (construct $APP_{346-548}$) have been described previously.[19] Full-length cDNA for human APLP1 was purchased from Open Biosystems (MHS1010-74392). A total of six E2 constructs of APLP1 were made on the basis of sequence alignment with APP.[19] They differed from each other by a few amino acids at either the N- or C-terminus. The constructs were subcloned into vector pET28a (Novagen) at the NdeI and XhoI restriction sites. Recombinant protein was expressed in BL21-Gold(DE3) cells (Agilent Technologies) grown in LB medium. After induction with 0.5 mM IPTG at an OD_{600} of 0.5, the cell culture was continued for 18 h at room temperature. Harvested cells were resuspended in a buffer containing 20 mM sodium phosphate (pH 7.8), 500 mM sodium chloride, and complete protease inhibitor cocktail (Roche) and lysed by being frozen and thawed in the presence of lysozyme. The recombinant protein was purified from the lysate using Talon affinity chromatography (Clontech). The N-terminal hexahistidine tag was removed by thrombin after overnight dialysis of the recombinant protein against gel filtration buffer [20 mM HEPES (pH 7.5), 500 mM NaCl, and 5% glycerol]. Thrombin-treated protein was concentrated and passed through a Superdex S-200 column (GE Healthcare). The monodispersed peak was collected for later studies. Mutants were generated by the QuikChange method of site-directed mutagenesis according to the protocol supplied by the manufacturer (Agilent Technologies). They were expressed and purified similarly.

Crystallization and Determination of the Structure of APP. Platelike crystal clusters could be readily generated by the hanging drop method by mixing 1 μL of a 10 mg/mL protein solution in a buffer of 10 mM HEPES (pH 7.5) with 1 μL of a well solution consisting of 12% PEG 4000, 20% 2-propanol, and 0.1 M sodium citrate (pH 5.6). Single crystals were cut from the cluster and cryoprotected in 30% PEG 400. The native crystal diffracted to 3.2 Å resolution, but the diffraction was anisotropic and tended to produce streaky spots. After many crystals had been screened, a complete native data set was collected from a single and best-diffracting crystal to 3.4 Å resolution.

The molecular replacement program *phaser*[26] found a clear solution by using two search models, each presenting the N- and C-terminal subdomains of the known E2 structure [Protein Data Bank (PDB) entry 1rw6]. Refinement was, however, difficult as the electron density map showed very few new features based on which the model could be improved (the initial *R* factor was around 0.47). Density modification was not useful because the solvent content of the crystal was normal (~51%) and there was no noncrystallographic symmetry averaging. After rounds of refinement, the *R* and R_{free} values remained high (0.41 and 0.44, respectively). We decided then to try to obtain experimental phases. The Se-Met-substituted protein turned out to produce slightly better diffracting crystals, and cryoprotection with paratone oil was found to be better and more reproducible. Two highly redundant Se-MAD data sets were collected. Unfortunately, they failed to generate useful phase information even with the known Se sites, which could be obtained from the molecular replacement solution. We noticed that our crystallization condition was similar to that reported by Keil et al., who were successful in derivatizing APP crystals with $(NH_4)_2OsCl_6$ (their protein construct was longer and crystallized in a different space group).[23] We soaked our Se-Met crystals in 5 mM $(NH_4)_2OsCl_6$ overnight before transferring them to paratone oil and flash-freezing them in liquid nitrogen. A 3.2 Å resolution data set was collected at the Os peak wavelength (1.1400 Å) at beamline X29 of BNL-NSLS. *hkl2map*[27] was able to find the single Os site, but the electron density map based on SAD phasing was again not interpretable. Because of the lack of isomorphism, the attempt to obtain phases by SIRAS, using the Os data and a "native" Se-Met data set collected at the same wavelength, also failed. Because the 3.2 Å resolution Os data set was better in quality than the earlier native data set and produced clearer maps, we used it to conduct molecular replacement and refinement again. This time we used an ensemble of three structures (APP, APL-1, and APLP1) that have now become available to emphasize features common to this family of proteins. The first short helix αA was removed from the N-terminal search probe because of clashes with a neighboring molecule. *phaser* found the same molecular replacement solution, but the resulting electron density map was more meaningful, revealing many differences between the real structure and the search probe. To ensure that the molecular replacement solution was correct, a difference anomalous Fourier map was calculated from a data set collected from a Se-Met crystal at the Se peak wavelength (0.9792 Å), which revealed strong peaks that matched perfectly with six of the nine methionines in E2 predicted by the molecular replacement solution (Figure S1 of the Supporting Information). The peaks were of different heights (the two N-terminal methiones were 8σ above background), reflecting different degrees of motion. At 4σ, no other peaks were visible in the map. An anomalous difference Fourier map calculated from the Os data set revealed a single 14σ peak situated between the two subdomains of E2 that corresponded to the bound metal ion (Figure S2A of the Supporting Information). The coordinates of the bound Os (−0.5726, 0.1249, 0.2758) were consistent with peaks observed in an anomalous Patterson map, which was independently calculated (Figure S2B of the Supporting Information). Figure S3 of the Supporting Information compares a region of the electron density map showing how helices αD and αE are differently connected in the new structure: a poorly defined and extended segment from His-495 to Met-498 had now become a continuation of the αD helix; to bridge the gap between the two helices, a short segment of helix αE, from Pro-501 to Gln-506, had bent sharply toward αD, creating a kink after Gln-506. The new structure was now more similar to that of APLP1 in this region (both had the kink after Gln-506). The model had an *R* factor initially around 0.46. After cycles of refinement with *CNS* and *refmac5*,[28,29] and manual adjustments using *O*[30] based on $2F_o - F_c$ and $F_o - F_c$ maps, we refined the structure to *R* and R_{free} values of 0.29 and 0.37, respectively, with reasonable geometry (Table 1). Further improvement was hindered by resolution and by disorder that appeared to be intrinsic to this crystal form, which rendered some parts of the structure difficult to visualize. The overall temperature factor was high (102 Å^2). Electron density was particularly poor near the two termini (αA and αF) and in the loop between αC and αD. Approximately 20% of the side chains remained missing in the final electron density map.

A comparison with the high-resolution APLP1 structure (see below) suggested that a few changes need to be made to the original APP structure, which was also determined at a medium to low resolution.[19] The changes involved the ends of the molecule that were poorly defined in the electron density map.

Table 1. Crystallographic Statistics

	APP (crystal form B)	APLP1
	Data Collection	
space group	$P2_12_12$	$P2_12_12_1$
cell dimensions (Å)	a = 115.0, b = 40.1, c = 58.4	a = 74.9, b = 81.3, c = 89.7
wavelength (Å)	1.1400	1.075
resolution[a] (Å)	40.0−3.2 (3.31−3.20)	40.0−2.1 (2.18−2.10)
no. of observed reflections	65248	303135
no. of unique reflections	4888	32194
redundancy	13.3	9.4
completeness[a] (%)	99.6 (100.0)	100.0 (100.0)
$\langle I/\sigma \rangle$[a]	14.0	16.5
R_{merge}[a,b]	0.081 (0.368)	0.070 (0.402)
	Refinement	
resolution (Å)	40.0−3.2	40.0−2.1
R_{work}/R_{free}[c]	0.297/0.380	0.208/0.244
no. of atoms		
protein	1226	3170
metal ion	1	0
phosphate ion	0	20
water	36	277
B factor		
protein	110	46
metal ion	92	−
phosphate ion	−	56
water	101	55
root-mean-square deviation		
bond lengths (Å)	0.009	0.007
bond angles (deg)	1.57	1.06

[a] Data for the highest-resolution shell are given in parentheses. [b] $R_{merge} = \Sigma|I_i - \langle I \rangle|/\Sigma I_i$. [c] $R_{work} = \Sigma|F_o - F_c|/\Sigma F_o$. R_{free} is the cross-validation *R* factor for the test set of reflections (10% of the total) omitted from model refinement.

Near the N-terminus, the loop between helices αA and αB was rebuilt so that Tyr-359 now pointed inward to form hydrogen bonds with Glu-368 and Arg-441. Toward the C-terminus, a remodeled loop before helix αF would allow Ile-539 to make hydrophobic contacts with Val-471, Phe-472, and Leu-529. After the changes had been incorporated, the R and R_{free} values of the model improved from 0.274 and 0.342 to 0.258 and 0.322, respectively. The improved coordinates have also been deposited as PDB entry 3NYL.

Crystallization and Structural Determination of APLP1. Crystallization conditions were initially screened in 96-well sitting drop plates using commercial kits Crystal Screen, Index, SaltRx, PEG/Ion (Hampton Research), and Wizard (Emerald Biosystems). All six constructs produced crystals, most of which showed the morphology of needle clusters. After optimization, single rodlike crystals were obtained from construct $APLP1_{285-499}$ when a 7 mg/mL protein solution in 20 mM HEPES (pH 7.5) and 5% glycerol was mixed with an equal volume of well solution containing 1.26 M Na_2HPO_4 and 0.14 M KH_2PO_4 (pH 5.6) and equilibrated for 4−7 days using the sitting drop vapor diffusion method. The crystals were cryoprotected in 100% Paratone-N (Hampton Research) before being flash-frozen in liquid nitrogen. X-ray diffraction data were acquired at Brookhaven National Synchrotron Light Source beamline X29 and processed with *HKL2000*.[31] The structure was again determined with *phaser*: because there were two copies of E2 in the asymmetric unit, and the two subdomains in each polypeptide chain were flexible, the program had to locate four search models (both subdomain models were an ensemble of human APP and worm APL-1 structures).[19,25] The model phase was significantly improved by the independent 2-fold averaging of the N- and C-terminal subdomains (the symmetry operators for the two subdomains were different by 5°). On the basis of the density-modified map, an almost complete model for APLP1 could be confidently built (including retracing of the domain-swapped loop and helix αA) using *coot*.[32] After two rounds of model building and refinement by *CNS*,[28] R and R_{free} decreased to 0.286 and 0.308, respectively. At this stage, the difference map was inspected, which clearly revealed four bound phosphate ions (Figure S7 of the Supporting Information). Adding the phosphate ions to the protein model, and autopicking water molecules, further reduced the R value and improved the clarity of the map. The final step of refinement was conducted using *refmac5*[29] (Table 1).

Analytical Ultracentrifugation. All experiments were performed on a Beckman Optima XL-I instrument at the Center for Analytical Ultracentrifugation of Macromolecular Assemblies (CAUMA) at the University of Texas Health Science Center at San Antonio. Sedimentation velocity (SV) data were analyzed with *UltraScan*.[33,34] Calculations were performed at the Texas Advanced Computing Center at the University of Texas at Austin and at the Bioinformatics Core Facility at the University of Texas Health Science Center at San Antonio as described in ref 35. Both APP and APLP1 were prepared in a buffer containing 10 mM sodium phosphate, 10 mM sodium acetate, and 50 mM NaCl (pH 7.5). The protein−heparin complexes were prepared in the same buffer with 100 μM heparin [average molecular mass of 5000 Da (Santa Cruz Biotechnology)]. The data were measured in intensity mode at 230 and 280 nm, 20 °C, and 45K rpm, using standard Epon two-channel centerpieces. The protein concentrations for samples measured at 230 nm were ~3.2 μM (OD_{230} = 0.31); those measured at 280 nm ranged from 28 μM (OD_{280} = 0.32) to 66 μM (OD_{280} = 0.76). Partial specific volumes of APP and APLP1 were determined to be 0.729 and 0.728 cm^3/g, respectively. Data were first analyzed by two-dimensional spectrum analysis with simultaneous removal of time-invariant noise[36,37] and then by enhanced van Holde−Weischet analysis[38] and genetic algorithm refinement,[39,40] followed by Monte Carlo analysis.[41]

Fluorescence Spectroscopy. The fluorescence measurements were performed using a spectrofluorometer from Photon Technology International. The excitation wavelength was set at 295 nm, and the emission spectra were recorded from 300 to 450 nm with a 1 nm interval at a speed of 1 nm/s. A total of three scans were acquired and averaged. The protein solutions were in 20 mM phosphate buffer (pH 7.5), and the protein concentration was 3 μM. The protein−heparin complexes were prepared in the same buffer with 6 μM heparin [average molecular mass of 5000 Da (Santa Cruz Biotechnology)]. The emission spectra of free tryptophan, which were recorded similarly, were not affected by the presence of heparin.

Heparin Affinity Chromatography. All protein samples were dialyzed against a buffer containing 10 mM sodium phosphate and 10 mM sodium acetate (pH 7.5). The protein sample was applied to a 1 mL Hi-Trap Heparin HP column (GE Healthcare) equilibrated with the same buffer and eluted with a linear concentration gradient (from 0.0 to 2.0 M) of NaCl.

RESULTS

Structure of the APP E2 Domain in a New Crystal Form. To address the question of whether the E2 dimer observed in the previous APP structure could result from crystallization, we have now found a new crystal form of APP (crystal form B), which is based on a slightly shorter E2 construct and was obtained from a different crystallization condition (polyethylene glycol instead of salt). The new structure was determined by molecular replacement (Table 1). Although poor diffraction and disorder had rendered refinement difficult, the molecular replacement solution has to be correct: it can be used to accurately locate six of the nine selenium atoms, and an osmium atom, from Se-Met- and Os-derivatized crystals by anomalous Fourier analysis using diffraction data collected at Se or Os absorption edges (Figures S1 and S2 of the Supporting Information); it also produces clear electron densities for parts of the protein structure that are either disordered or different in the search probe (Figure S3 of the Supporting Information). One polypeptide chain is present in the asymmetric unit of the crystal. It is closely packed against a second molecule related by crystallographic 2-fold symmetry to form a dimer, in an antiparallel manner similar to that observed in the first crystal form (Figure 1B). The antiparallel dimers, now observed twice, and their overall similarities cannot be coincidental, especially when their crystal packing environments are completely different. In the following sections, we will describe a third E2 dimer structure (that of APLP1), which is determined at a much better resolution and properly refined, and show that it not only shares the same mode of dimerization but also demonstrates similar conformational flexibilities.

Structure of the APLP1 E2 Domain. The E2 domain of APLP1 is 51% identical in sequence with the E2 domain of APP (Figure S4 of the Supporting Information). Assisted by multidomain averaging, its structure can also be determined by molecular replacement (Table 1): the electron density map

calculated after density modification was of very high quality, revealing most of the differences between APLP1 and the search probe; it also became clear that the first α-helix (αA) of both copies of E2 in the asymmetric unit is domain-swapped with a neighboring molecule (Figure S5A,B of the Supporting Information). In the two previously known E2 structures,[19,25] αA is packed to the side of αB and αC, which brings together four completely conserved residues (Tyr-297, Glu-306, His-376, and Arg-379) to form a network of hydrogen bonds (Figure S5C, D of the Supporting Infomation). All these interactions are maintained in the domain-swapped APLP1 structure (with the exception that Tyr-297 now comes from a separate polypeptide chain). The swapping is made possible by two glycyl residues and one prolyl residue in the short loop that connects αA to αB. Most illustrations of APLP1 in this paper have αA modeled back to its original position.

There are two copies of E2 in the asymmetric unit of the APLP1 crystal that are related roughly by a 2-fold rotation (Figure 1C). The two E2 domains form a tightly associated dimer that is quite similar to the E2 dimer of APP described above. The corresponding helices in the two E2s are pointing in opposite directions, and the N-terminal subdomain of one monomer is packed against the C-terminal subdomain of the second monomer, burying an identical set of conserved hydrophobic residues (see below). Helices αB and αC in APLP1, however, are more tilted outward. This is accompanied by rotations of αD and αE in its dimerization partner to maintain contact. As a result of these movements, the dimeric structure of APLP1 appears less compact and contains a large hole in the middle that connects the front of the molecule to the back.

Conformational Flexibilities within the Monomer. When the two APP structures are superimposed on the C-terminal subdomain, the N-terminal subdomain of the new structure appears to have bent significantly outward by about 15° (Figure 2A). The flexibility is achieved by small dihedral angle changes in a short stretch of residues around Arg-441 near the middle of the long αC helix. Because there is little contact between the two subdomains within the monomer (the only interaction lost in the new structure is a hydrogen bond between Glu-436 and His-492), their relative orientation has to be maintained by the continuity of the long helix αC that spans the length of the molecule. The fact that Arg-441 can be partially cleaved by trypsin in solution [when the molecule is monomeric (see below)] suggests that the long helix can sometimes unwind in the middle, which would probably allow the N-terminal subdomain to bend further than illustrated by the current structures.[24]

The structures of the two subdomains in APLP1 are very similar to those in APP: their helices (63 Cα atoms from the N-terminal subdomain and 74 Cα atoms from the C-terminal subdomain) are superimposable with root-mean-square deviations (rmsds) of 0.70 and 1.08 Å, respectively. The largest difference between APLP1 and APP is again in the intersubdomain angle: the N-terminal subdomain of APLP1 is tilted further away from the C-terminal subdomain by ~31° (black and red in Figure 2B). The two copies of E2 in the asymmetric unit of the APLP1 crystal are not exactly identical: they differ also in the intersubdomain angle by ~5° (black and blue in Figure 2B).

Conformational Flexibilities within the Dimer. Despite the large movement between the two subdomains (Figure 2A), the dimerization interface is maintained. Figure 3A compares the two APP structures at one of the two identical interfaces (the region boxed in Figure 3C), where the N-terminal helical hairpin (αB and αC) crosses over a pair of C-terminal helices (αD and αE): via superimposition of the structures on the C-terminal helices, αB and αC of the new structure appear to have rotated downward, creating a wider gap with αD and αE. Most interactions at the interface are changed by this movement with the exception of the hydrophobic contacts between a pair of highly conserved

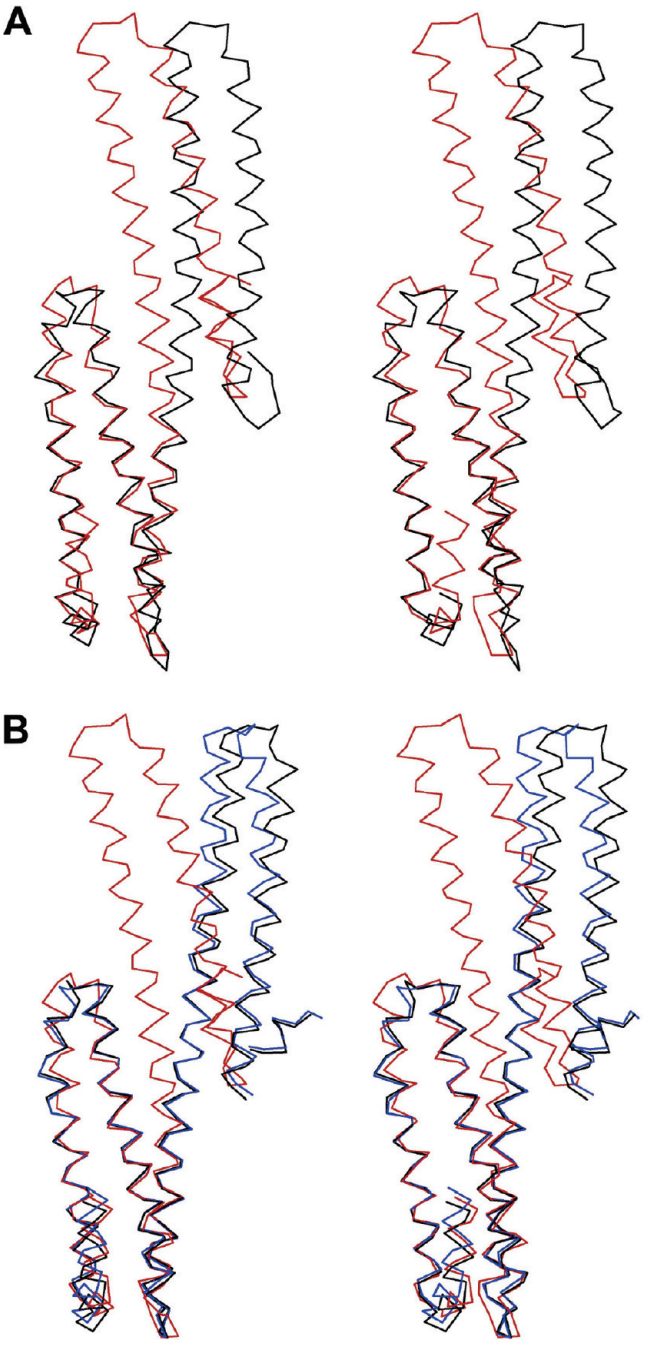

Figure 2. Differences at the tertiary structural level. (A) Comparison between the two APP crystal forms. The new structure (black) is superimposed onto the C-terminal subdomain of the original APP structure (red; PDB entry 1rw6). The Cα traces are shown as stereo pairs. (B) Comparison between APP (red; the original structure being PDB entry 1rw6) and APLP1 (blue and black). The two copies of APLP1 in the asymmetric unit are slightly different in their intersubdomain angles. These images and those in panels A and B of Figure 3 were generated with *Molscript*.[48]

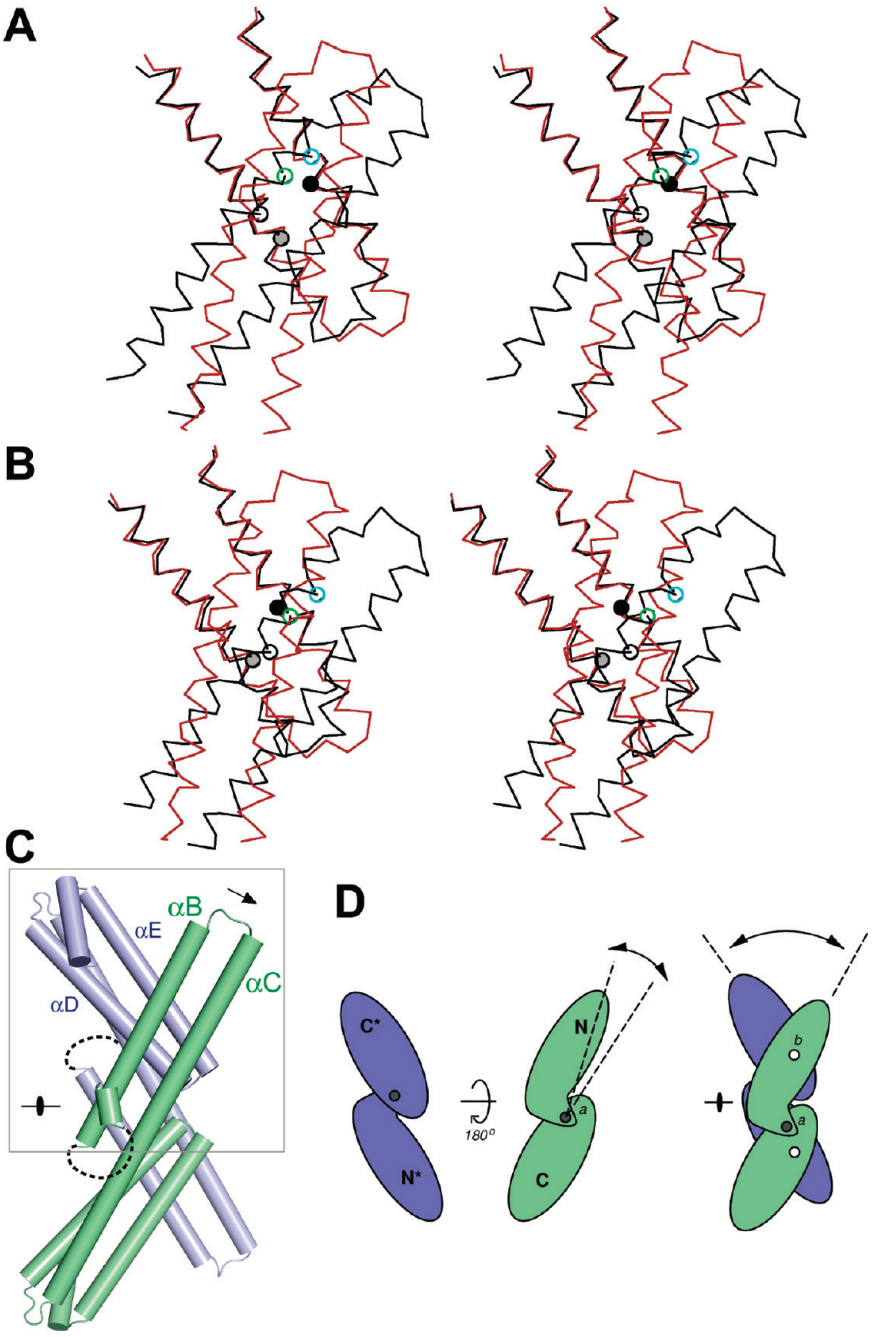

Figure 3. Differences at the dimeric interface. (A) Comparison between the two APP crystal forms. The new structure (black) is superimposed onto αD and αE of the original structure (red; PDB entry 1rw6). The helices that "moved" correspond to αB and αC of the second protomer across the dimeric interface. The Cα traces are shown as stereo pairs: (gray circle) Leu-490*, (black circle) Leu-515*, (white circle) Met-387, (green circle) Met-391, and (blue circle) Trp-394. αB and αC appear to pivot around Met-387. (B) Comparison between APP (red; the original structure being PDB entry 1rw6) and APLP1 (black): (gray circle) Leu-428*, (black circle) Leu-453*, (white circle) Ile-325, (green circle) Met-329, and (blue circle) Trp-332. (C) Side view of the APLP1 dimer. The arrow indicates the "rotation" of αB and αC relative to αD and αE across the dimeric interface in APLP1 when compared to APP. The gray box indicates the region shown in panels A and B. (D) In this model, each subdomain is represented by a single oval-shaped object. Within each protomer, the two subdomains are connected at point "a" (gray circle) and can rotate about it (———). The dimer is held together by two joints (white circles, "b"). The two subdomains across the dimeric interface can only rotate about "b" (———).

leucines (Leu-490* and Leu-515*) on αD and αE and a string of three hydrophobic residues (Met-387, Met-391, and Trp-394) on αB. The lack of any strong interactions may account for the flexibility observed at the interface.

The bending of the N-terminal subdomain at the tertiary structural level and the rotation at the dimeric interface are mechanically coupled (Figures 2A and 3A). The movements of individual subdomains within the dimer can be simulated by the model depicted in Figure 3D. In this model, the subdomains from the two monomers are joined at "b" (open circle) and can only rotate about it. Any rotation around "a" (gray circle) inevitably leads to a rotation around "b", in the direction that is

dx.doi.org/10.1021/bi101846x |*Biochemistry* 2011, 50, 5453–5464

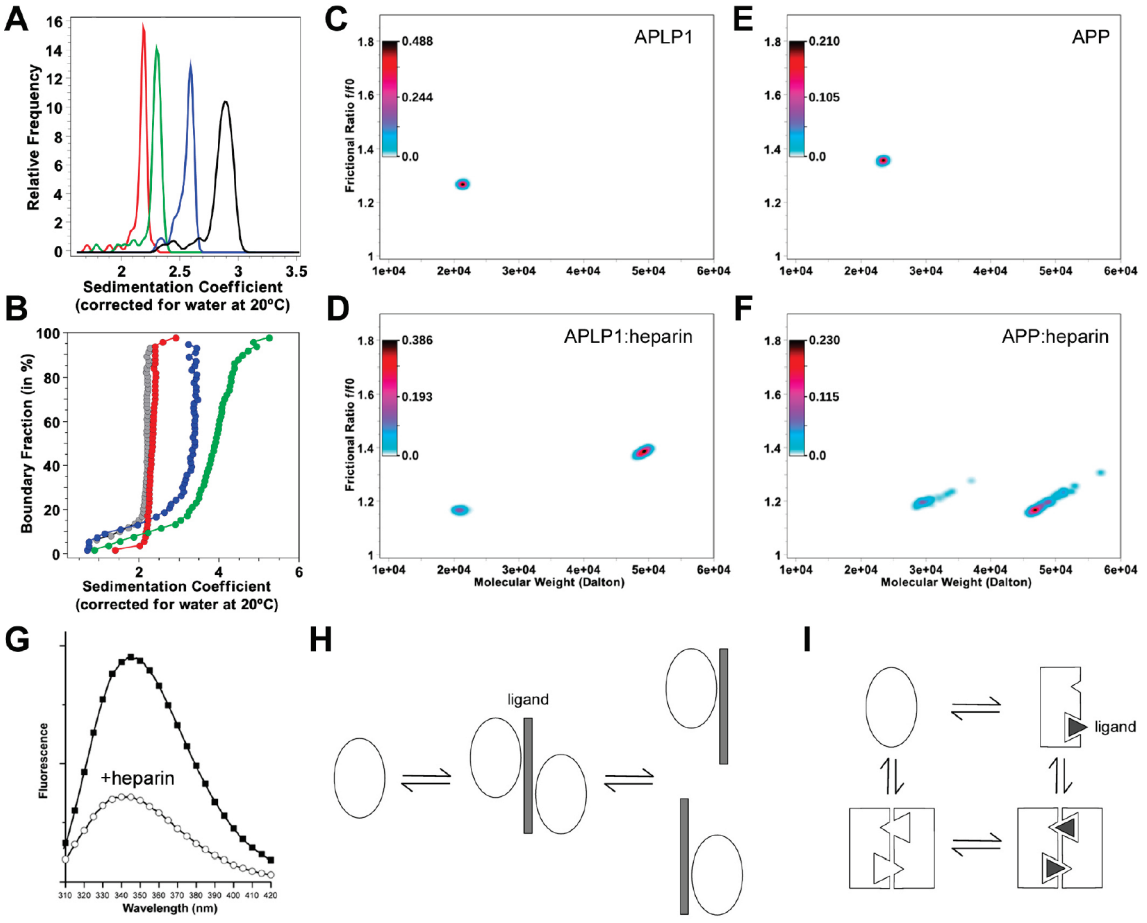

Figure 4. Heparin binding enhances E2 dimerization. (A) van Holde−Weischet $g(s)$ graphs for the E2 domain of APLP1 for a range of protein concentrations (red, 3.2 μM; green, 6.6 μM; blue, 32 μM; black, 66 μM). When the protein concentration was increased from 3.2 μM (OD_{230} = 0.31) to 66 μM (OD_{280} = 0.76), the major peak gradually shifted from 2.2 to 2.9 S. This result is due to the rapid exchange between monomers (24.9 kDa) and dimers (49.8 kDa) and was confirmed by fitting the data to a reversible monomer−dimer model.[42,43] This observation suggests that reversible dimerization is driven by mass action even in the absence of ligand. (B−F) Sedimentation velocity experiments with the E2 domains of APLP1 and APP in the presence and absence of heparin. Integral van Holde−Weischet s value distributions [(B) gray, APLP1; blue, APLP1 with 100 μM heparin; red, APP; green, APP with 100 μM heparin] and genetic algorithm−Monte Carlo results [(C) APLP1, (D) APLP1 with 100 μM heparin, (E) APP, and (F) APP with 100 μM heparin] reveal enhanced dimerization when heparin is present. In panels C−F, the y-axis shows the frictional ratio (f/f_0), which measures the globularity of the solute. An f/f_0 value of unity corresponds to a spherical molecule. The color gradients indicate the optical density at 230 nm. For the sake of clarity, only the monomer−dimer molecular weight range is shown in panels C−F. The full sedimentation range is shown in panel B. The protein loading concentration is approximately 3 μM in all experiments shown in panels B−F. (G) Heparin binding causes a decrease in APLP1 E2 fluorescence intensity: (●) protein alone (3 μM) and (○) protein with heparin (6 μM). (H) Model in which the heparin-induced dimer does not have a protein−protein interface. Additional ligand may dissociate the dimer by competing for the ligand binding site: oval, protein; gray bar, ligand. (I) In this model, the dimer is strengthened by protein−protein contact and by additional interactions between heparin (represented by the gray triangles) and the protein protomer across the dimeric interface (small indentation). Ligand may also change the conformation of the protein (oval to rectangle) to facilitate the formation of a protein−protein interface.

consistent with the crystallographic observation. In the real structure, the contact between Met-387 and Leu-490*, which remains unchanged in the two structures (αB and αC appear to pivot around Met-387), would be equivalent to point "b" in the model.

The "movement" of helices in APLP1, when compared to APP, is strikingly similar to that between the two APP crystal forms [except that the difference is larger (Figure 3B)]. As also shown in Figure 3C, the N-terminal and C-terminal subdomains of APLP1 are similarly packed but have a wider angle between them. The dimeric interface involves an identical pair of conserved leucines on αD and αE (Leu-428* and Leu-453* in APLP1 numbering). Although αB has now moved to the lower side of the leucines, Ile-325 and Met-329 (equivalent to Met-387 and Met-391, respectively, of APP) remain in hydrophobic contact with them. These comparisons suggest that individual subdomains in the APLP1 dimer structure are similarly coupled so that, during the course of evolution, their movements are restrained by the same type of requirements to maintain dimeric contact.

Heparin Binding Alters the E2 Monomer−Dimer Equilibrium. The oligomeric structure of the E2 domains in solution was studied by analytical ultracentrifugation (AUC), using sedimentation velocity (SV) experiments as described in ref 42. A concentration series of APLP1 was analyzed with the enhanced van Holde−Weischet method[38] and revealed a mass-action effect suggesting the presence of a monomer−dimer equilibrium (Figure 4A): while essentially monomeric at 3 μM, at 66 μM the s value distribution was shifted considerably to the dimeric state.

dx.doi.org/10.1021/bi101846x |*Biochemistry* 2011, 50, 5453–5464

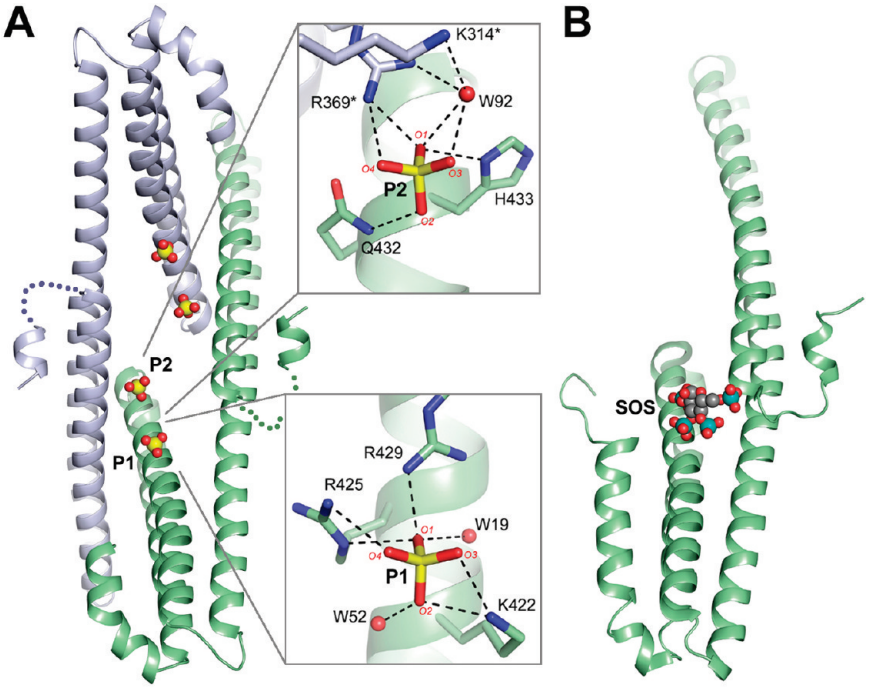

Figure 5. Phosphate binding sites. (A) P1 and P2 binding sites. Dashed lines represent hydrogen bonds. Red spheres represent water molecules. The two protein protomers are shown in different colors. (B) Similar view of the monomeric structure of *C. elegans* APL-1 in complex with sucrose octasulfate.[25]

Whole boundary modeling of two separate high-concentration experiments with a reversible model for the Lamm equation[43] as described in ref 42 resulted in two equivalent fits, which indicated a weak but rapidly reversible monomer−dimer equilibrium [K_d = 161 μM (144.2, 182.7); $k_{off} \geq 0.003$ s^{-1}]. Heparin altered this equilibrium significantly. Even at 3 μM E2, the presence of 100 μM heparin shifted the van Holde−Weischet integral *s* value distributions, suggesting higher oligomerization states (Figure 4B). Plots of genetic algorithm−Monte Carlo analyses using noninteracting models for these data clearly show an increase in the partial concentration of a higher-molecular mass species, which is consistent with the formation of E2 dimers (Figure 4C−F). To further quantify the degree of this association, we fitted the heparin data to reversible monomer−dimer association models as described in ref 42. These fits resulted in K_d values of 9.2 μM (8.1, 10.7) for APP and 7.8 μM (6.8, 9.3) for APLP1, suggesting a dimerization significantly tighter than that observed for APLP1 without heparin. Taken together, these analyses demonstrated for the first time that heparin binding to E2 shifts the association−dissociation equilibrium in favor of dimer formation and confirmed our earlier hypothesis that E2 dimerization is a dynamic and reversible process.[19,25]

The E2 domain of APLP1 contains a single tryptophan residue (Trp-332). Adding heparin to the protein solution causes a 60% decrease in the protein's fluorescence intensity (Figure 4G). This effect is specific to heparin because other polyanions such as sucrose octasulfate (a heavily sulfated disaccharide) and chondroitin sulfate (which is similar to heparan sulfate but has galactosamine residues instead of glucosamines in its backbone) do not change the protein's fluorescence properties (Figure S7 of the Supporting Information). Because Trp-332 is far from the known heparin binding site on E2, thus unlikely to be directly affected by the ligand, the change in its fluorescence property must result from protein dimerization (or a conformational change that is associated with dimerization). This is consistent with the observation that Trp-332 is found at the dimeric interface of the crystal structures (blue empty circles in Figure 3B). The binding of heparin to APP also causes a change in protein fluorescence, but the amplitude of the change is smaller (data not shown).

Heparin may induce protein dimerization through at least one of two possible mechanisms. In one mechanism, the protein protomers are bridged by the ligand but do not interact with each other directly (Figure 4H). This is possible especially because heparin is a linear polymer with many repeating disaccharide units and both sides of the sugar can bind proteins. At higher ligand concentrations, however, the dimer is expected to break apart readily so that each protein protomer can bind a separate ligand molecule. In the second mechanism, dimerization involves extensive protein−protein contact (Figure 4I). Heparin binding may modify the surface property of the monomeric protein, rendering it complementary for dimer formation. The AUC experiments depicted in panels D and F of Figure 4 were conducted in the presence of an excessive amount of heparin (~30 times the protein concentration). The fact that the complex was mostly dimeric under this condition seems to suggest that the heparin-induced E2 dimer is stabilized by not only protein−heparin but also protein−protein interactions (Figure 4I).

The influence of heparin on E2 dimerization can be envisioned in a different but thermodynamically equivalent way (Figure 4I). E2 may dimerize in the absence of heparin, although equilibrium favors dissociation. If the ligand has a higher affinity for the dimeric E2, its presence will deplete the empty dimers and re-establish the equilibrium by drawing more monomers into dimers. The crystallization process, which takes place at high protein concentrations, may similarly favor the formation of dimers.

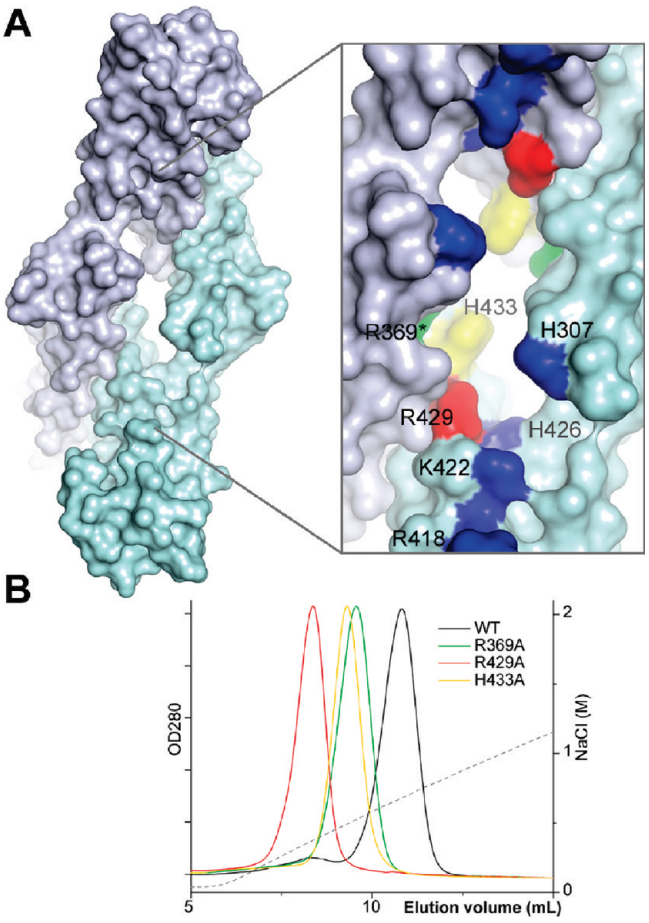

Figure 6. Mutational mapping of the heparin binding site. (A) Surface representation of the heparin binding site mapped by mutagenesis. The two protein protomers are shown in different colors. (B) Elution profiles of wild-type and mutant proteins from a heparin column. The dashed line represents a salt gradient.

Phosphate Binding Sites. The two previously determined E2 structures were of only medium resolution.[19,25] The high resolution of the APLP1 structure permits not only visualization of most protein side chains but also accurate modeling of bound solvent molecules. In the difference Fourier map, there are four prominent peaks [7−11σ (Figure S6 of the Supporting Information)]. These peaks are related roughly by the noncrystallographic 2-fold symmetry and appear next to positively charged protein side chains. They must correspond to heavier phosphate ions, which are abundantly present in the crystallization solution (the protein is crystallized in 1.4 M Na/K phosphate). One phosphate (P1) interacts with Lys-422, Arg-425, and Arg-429 from helix αD, and the second phosphate (P2) is hydrogen bonded to His-433 and Gln-432 from the same helix and to Lys-314* (via a water) and Arg-369* from the dimerization partner (Figure 5A). The proximity of the bound phosphates to previously mapped heparin binding site led us to test whether the phosphate binding sites are also involved in heparin binding [Lys-422 is already known to bind heparin (see refs 19 and 25)] (Figure 5B). Arg-429, His-433, and Arg-369 were chosen for mutagenesis because they are highly conserved and interact directly with the phosphates. As shown in Figure 6B, R429A, H433A, and R369A all elute earlier from a heparin column than the wild-type protein, confirming that these residues indeed participate in heparin binding.

The finding that heparin may interact with residues at the P2 binding site was not expected. Our previous work established that His-307, His-426, Arg-418, and Lys-422 are involved in heparin binding (colored blue in Figure 6A).[25] The shallow pocket defined by these residues is readily accessible from the front of the molecule (Figure 5B). The P2 binding site, however, is located much deeper toward the back of the molecule (yellow and green in Figure 6A). To reach the P2 binding site from the front, the bulky heparin chain has to go through the narrow space between the two subdomains. It is therefore tempting to speculate that the binding of heparin to the deep groove between the two subdomains may restrict their rotational freedom and thereby promote dimerization. The simultaneous binding of heparin to residues from both polypeptide chains (e.g., His-433 and Arg-369*) may also directly strengthen the dimeric interface. To test this hypothesis, we examined the dimerization effect of heparin on the three mutant proteins generated above. As shown in Figure 7A−C, when heparin was added to the protein solutions, the decrease in fluorescence intensity for the mutant proteins was smaller than that for the wild-type protein, suggesting a lesser degree of dimerization. Among the three mutants, R429A had the lowest affinity for heparin (Figure 6B), and under our experimental conditions, heparin almost completely failed to induce its dimerization (Figure 7B).

DISCUSSION

We draw three general conclusions about the oligomeric structure of E2 from this study. First, E2 can reversibly dimerize in solution. In the absence of ligand, however, the monomer predominates thermodynamically. This is probably true for all APP family members (ref 25 and our unpublished data). The techniques we used previously to analyze the oligomeric structure of E2 (size exclusion chromatography, dynamic light scattering) were inaccurate because the molecule has a very elongated shape.[19] The new conclusion is consistent with the observation made by Gralle et al. showing that the secreted APP ectodomain as a whole, which contains not only E2 but also other domains, is also monomeric in solution.[21] Second, we show for the first time that heparin binding causes E2 to dimerize. The dimerization of APP at the E2 domain can have many types of functional consequences. For example, dimerization may mask epitopes that potentially have biological activities. In the dimer structure, the RERMS sequence motif (APP_{751} residues 384−388), previously found to have growth promoting activities in cell culture,[7,44,45] and a possible collagen binding site (residues 504−521)[46] are buried at the interface and not available for interaction with other proteins. The dimerization of the membrane-spanning APP (or its dissociation) may also serve as a mechanism for sending signals into cells.[14] Third, the E2 domains appear to share a conserved mode of dimerization. This is based primarily on the crystallographic observation that, of the four E2 structures determined to date, three are dimeric and have similar structures. Only the E2 domain of the worm APL-1 was crystallized as monomers.[25] Furthermore, we showed that residues located at the dimer interface are highly conserved.[19]

We cannot yet explain how heparin binding induces E2 dimerization. The most straightforward approach to address this question would be to try to cocrystallize the E2−heparin complex, but this effort has not been successful. On the basis of

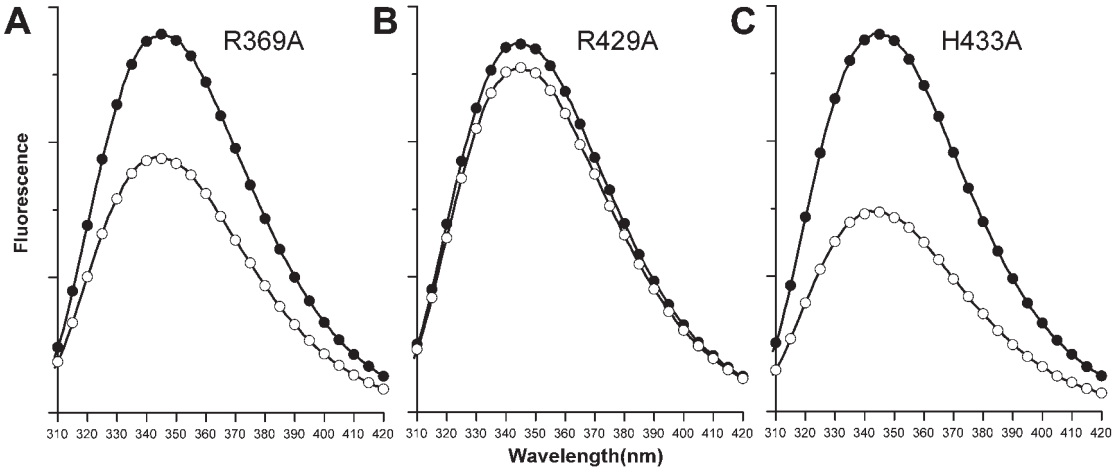

Figure 7. Heparin-binding mutants show decreased levels of dimerization. (A) R369A, (B) R429A, and (C) H433A. These experiments were conducted under exactly the same conditions that were used for the wild-type protein (Figure 4G): (●) mutant protein alone and (○) protein with heparin.

the hypothesis illustrated by Figure 4I, one may predict that the crystallized E2 dimer should represent the form of the protein that has a higher affinity for the ligand. Therefore, direct soaking of heparin into the protein crystal offers another possible solution to the problem. The present crystallization condition for APLP1 (1.4 M Na/K phosphate) prohibits heparin binding. We recently found a new condition for crystallizing APLP1 in polyethylene glycol, and preliminary X-ray diffraction analysis indicated that it also contains the dimeric protein. We are currently preparing this crystal form for a soaking experiment: if the dimer observed in the crystal is different from that induced by heparin binding in solution (we cannot yet rule out this possibility definitively), heparin may fail to bind to the protein or bind to a region of the protein that is inconsistent with the mutagenesis data.

Gralle et al. found that heparin induces dimerization of the full-length APP ectodomain.[21] The results we present here could be interpreted as an indication that the dimerization may take place at the centrally located E2 domain. Recently, however, Dahms et al. reported that heparin can also induce dimerization of the E1 domain,[20] which is located at the N-terminus of the full-length protein and separated from E2 by an acidic and probably unstructured segment of ~100 amino acids (and, in some isoforms, an additional small protease inhibitor domain). Although a small-angle X-ray scattering experiment has provided some general idea about the overall shape of the full-length molecule and its complex with heparin,[21] one has to caution that the relative positions of E1 and E2 cannot be accurately determined by this technique. Therefore, we cannot exclude the possibility that E1 and E2 may both contribute to dimerization in a cooperative manner (this is not entirely impossible because E1 and E2 are separated by a long and flexible linker). Because E2 appears to have a higher affinity for heparin,[47] there can even be speculation that it may represent the first site of protein−protein contact before E1 becomes involved.

■ ASSOCIATED CONTENT

Supporting Information. Anomalous Fourier maps for APP showing Se peaks and Os binding sites, electron density maps for the loop between αD and αE, a sequence alignment, an electron density map showing the domain-swapped feature of APLP1, the difference Fourier map showing the bound phosphate ions, and the fluorescence and AUC data of APLP1 in the presence of other polyanions (Figures S1−S7). This material is available free of charge via the Internet at http://pubs.acs.org.

Accession Codes

The atomic coordinates and structure factors (3NYJ and 3PMR) have been deposited in the Protein Data Bank (http://www.rcsb.org/).

■ AUTHOR INFORMATION

Corresponding Author

*Department of Pharmacology, Yale School of Medicine, 333 Cedar St., New Haven, CT 06520. Telephone: (203) 785-7530. Fax: (203) 785-7670. E-mail: ya.ha@yale.edu.

Present Addresses

[§]Monsanto Co., 700 Chesterfield Parkway West, Chesterfield, MO 63017.

Funding Sources

This work was supported by National Institutes of Health (NIH) Grant GM077547 (Y.H.). The ultracentrifugation analyses were supported in part by NIH Grant RR022200 (B.D.). Supercomputer allocations were provided by National Science Foundation Grant TG-MCB070038 (B.D.).

■ ACKNOWLEDGMENT

We thank J. Schlessinger for allowing us to use the spectrofluorometer in his laboratory. We also thank H. Robinson and A. Saxena at NSLS-X29 for assistance during X-ray diffraction data collection. Financial support for the beamline comes principally from U.S. Department of Energy and the National Institutes of Health. We thank Mr. Virgil Schirf for performing the AUC experiments at CAUMA, which is funded in part by the University of Texas Health Science Center at San Antonio (UTHSCSA) Cancer Therapy and Research Center through NIH-NCI P30 Grant CA054174, as well as by Texas State funds provided through the Office of the Vice President for Research of the UTHSCSA.

■ ABBREVIATIONS

APLP, APP-like protein; APP, amyloid precursor protein; AUC, analytical ultracentrifugation; GLPD, growth factor-like domain; SV, sedimentation velocity.

■ REFERENCES

(1) Bettens, K., Sleegers, K., and Van Broeckhoven, C. (2010) Current status on Alzheimer disease molecular genetics: From past, to present, to future. *Hum. Mol. Genet. 19*, R4–R11.

(2) Wasco, W., Bupp, K., Magendantz, M., Gusella, J. F., Tanzi, R. E., and Solomon, F. (1992) Identification of a mouse brain cDNA that encodes a protein related to the Alzheimer disease-associated amyloid β protein precursor. *Proc. Natl. Acad. Sci. U.S.A. 89*, 10758–10762.

(3) Wasco, W., Gurubhagavatula, S., Paradis, M. D., Romano, D. M., Sisodia, S. S., Hyman, B. T., Neve, R. L., and Tanzi, R. E. (1993) Isolation and characterization of APLP2 encoding a homologue of the Alzheimer's associated amyloid β protein precursor. *Nat. Genet. 5*, 95–100.

(4) Herms, J., Anliker, B., Heber, S., Ring, S., Fuhrmann, M., Kretzschmar, H., Sisodia, S., and Muller, U. (2004) Cortical dysplasia resembling human type 2 lissencephaly in mice lacking all three APP family members. *EMBO J. 23*, 4106–4115.

(5) Kang, J., Lemaire, H. G., Unterbeck, A., Salbaum, J. M., Masters, C. L., Grzeschik, K. H., Multhaup, G., Beyreuther, K., and Muller-Hill, B. (1987) The precursor of Alzheimer's disease amyloid A4 protein resembles a cell-surface receptor. *Nature 325*, 733–736.

(6) Hardy, J., and Selkoe, D. J. (2002) The amyloid hypothesis of Alzheimer's disease: Progress and problems on the road to therapeutics. *Science 297*, 353–356.

(7) Ninomiya, H., Roch, J. M., Sundsmo, M. P., Otero, D. A., and Saitoh, T. (1993) Amino acid sequence RERMS represents the active domain of amyloid β/A4 protein precursor that promotes fibroblast growth. *J. Cell Biol. 121*, 879–886.

(8) Quast, T., Wehner, S., Kirfel, G., Jaeger, K., De Luca, M., and Herzog, V. (2003) sAPP as a regulator of dendrite motility and melanin release in epidermal melanocytes and melanoma cells. *FASEB J. 17*, 1739–1741.

(9) Nikolaev, A., McLaughlin, T., O'Leary, D. D., and Tessier-Lavigne, M. (2009) APP binds DR6 to trigger axon pruning and neuron death via distinct caspases. *Nature 457*, 981–989.

(10) Cao, X., and Sudhof, T. C. (2001) A transcriptionally correction of transcriptively active complex of APP with Fe65 and histone acetyltransferase Tip60. *Science 293*, 115–120.

(11) Baek, S. H., Ohgi, K. A., Rose, D. W., Koo, E. H., Glass, C. K., and Rosenfeld, M. G. (2002) Exchange of N-CoR corepressor and Tip60 coactivator complexes links gene expression by NF-κB and β-amyloid precursor protein. *Cell 110*, 55–67.

(12) Pardossi-Piquard, R., Petit, A., Kawarai, T., Sunyach, C., Alves da Costa, C., Vincent, B., Ring, S., D'Adamio, L., Shen, J., Muller, U., St George Hyslop, P., and Checler, F. (2005) Presenilin-dependent transcriptional control of the Aβ-degrading enzyme neprilysin by intracellular domains of βAPP and APLP. *Neuron 46*, 541–545.

(13) Eggert, S., Midthune, B., Cottrell, B., and Koo, E. H. (2009) Induced dimerization of the amyloid precursor protein leads to decreased amyloid-β protein production. *J. Biol. Chem. 284*, 28943–28952.

(14) Gralle, M., Botelho, M. G., and Wouters, F. S. (2009) Neuroprotective secreted amyloid precursor protein acts by disrupting amyloid precursor protein dimers. *J. Biol. Chem. 284*, 15016–15025.

(15) Scheuermann, S., Hambsch, B., Hesse, L., Stumm, J., Schmidt, C., Beher, D., Bayer, T. A., Beyreuther, K., and Multhaup, G. (2001) Homodimerization of amyloid precursor protein and its implication in the amyloidogenic pathway of Alzheimer's disease. *J. Biol. Chem. 276*, 33923–33929.

(16) Soba, P., Eggert, S., Wagner, K., Zentgraf, H., Siehl, K., Kreger, S., Lower, A., Langer, A., Merdes, G., Paro, R., Masters, C. L., Muller, U., Kins, S., and Beyreuther, K. (2005) Homo- and heterodimerization of APP family members promotes intercellular adhesion. *EMBO J. 24*, 3624–3634.

(17) Munter, L. M., Voigt, P., Harmeier, A., Kaden, D., Gottschalk, K. E., Weise, C., Pipkorn, R., Schaefer, M., Langosch, D., and Multhaup, G. (2007) GxxxG motifs within the amyloid precursor protein transmembrane sequence are critical for the etiology of Aβ42. *EMBO J. 26*, 1702–1712.

(18) Kaden, D., Voigt, P., Munter, L. M., Bobowski, K. D., Schaefer, M., and Multhaup, G. (2009) Subcellular localization and dimerization of APLP1 are strikingly different from APP and APLP2. *J. Cell Sci. 122*, 368–377.

(19) Wang, Y., and Ha, Y. (2004) The X-ray structure of an antiparallel dimer of the human amyloid precursor protein E2 domain. *Mol. Cell 15*, 343–353.

(20) Dahms, S. O., Hoefgen, S., Roeser, D., Schlott, B., Guhrs, K. H., and Than, M. E. (2010) Structure and biochemical analysis of the heparin-induced E1 dimer of the amyloid precursor protein. *Proc. Natl. Acad. Sci. U.S.A. 107*, 5381–5386.

(21) Gralle, M., Oliveira, C. L., Guerreiro, L. H., McKinstry, W. J., Galatis, D., Masters, C. L., Cappai, R., Parker, M. W., Ramos, C. H., Torriani, I., and Ferreira, S. T. (2006) Solution conformation and heparin-induced dimerization of the full-length extracellular domain of the human amyloid precursor protein. *J. Mol. Biol. 357*, 493–508.

(22) Rossjohn, J., Cappai, R., Feil, S. C., Henry, A., McKinstry, W. J., Galatis, D., Hesse, L., Multhaup, G., Beyreuther, K., Masters, C. L., and Parker, M. W. (1999) Crystal structure of the N-terminal, growth factor-like domain of Alzheimer amyloid precursor protein. *Nat. Struct. Biol. 6*, 327–331.

(23) Keil, C., Huber, R., Bode, W., and Than, M. E. (2004) Cloning, expression, crystallization and initial crystallographic analysis of the C-terminal domain of the amyloid precursor protein APP. *Acta Crystallogr. D60*, 1614–1617.

(24) Dulubova, I., Ho, A., Huryeva, I., Sudhof, T. C., and Rizo, J. (2004) Three-dimensional structure of an independently folded extracellular domain of human amyloid-β precursor protein. *Biochemistry 43*, 9583–9588.

(25) Hoopes, J. T., Liu, X., Xu, X., Demeler, B., Folta-Stogniew, E., Li, C., and Ha, Y. (2010) Structural characterization of the E2 domain of APL-1, a *Caenorhabditis elegans* homolog of human amyloid precursor protein, and its heparin binding site. *J. Biol. Chem. 285*, 2165–2173.

(26) McCoy, A. J., Grosse-Kunstleve, R. W., Adams, P. D., Winn, M. D., Storoni, L. C., and Read, R. J. (2007) Phaser crystallographic software. *J. Appl. Crystallogr. 40*, 658–674.

(27) Pape, T., and Schneider, T. R. (2004) HKL2MAP: A graphical user interface for macromolecular phasing with SHELX programs. *J. Appl. Crystallogr. 37*, 843–844.

(28) Brunger, A. T., Adams, P. D., Clore, G. M., DeLano, W. L., Gros, P., Grosse-Kunstleve, R. W., Jiang, J. S., Kuszewski, J., Nilges, M., Pannu, N. S., Read, R. J., Rice, L. M., Simonson, T., and Warren, G. L. (1998) Crystallography & NMR system: A new software suite for macromolecular structure determination. *Acta Crystallogr. D54*, 905–921.

(29) Winn, M. D., Murshudov, G. N., and Papiz, M. Z. (2003) Macromolecular TLS refinement in REFMAC at moderate resolutions. *Methods Enzymol. 374*, 300–321.

(30) Jones, T. A., Zou, J. Y., Cowan, S. W., and Kjeldgaard, M. (1991) Improved methods for building protein models in electron density maps and the location of errors in these models. *Acta Crystallogr. A47* (Part 2), 110–119.

(31) Otwinowski, Z., and Minor, W. (1997) Processing of X-ray diffraction data collected in oscillation mode. *Methods Enzymol. 276*, 307–326.

(32) Emsley, P., Lohkamp, B., Scott, W. G., and Cowtan, K. (2010) Features and development of Coot. *Acta Crystallogr. D66*, 486–501.

(33) Demeler, B. (2005) UltraScan: A Comprehensive Data Analysis Software Package for Analytical Ultracentrifugation Experiments. In *Modern Analytical Ultracentrifugation: Techniques and Methods* (Scott, D., Harding, S., and Rowe, A., Eds.) pp 210−229, Royal Society of Chemistry, Cambridge, U.K.

(34) Demeler, B. (2010) UltraScan: A comprehensive data analysis software package for analytical ultracentrifugation experiments. http://www.utrascan.uthscsa.edu/.

(35) Brookes, E., and Demeler, B. (2008) Parallel computational techniques for the analysis of sedimentation velocity experiments in UltraScan. *Colloid Polym. Sci. 286*, 138–148.

(36) Brookes, E. H., Boppana, R. V., and Demeler, B. (2006) Computing large sparse multivariate optimization problems with an application in biophysics. In *Proceedings of the 2006 ACM/IEEE conference on Supercomputing*, p 81, ACM, Tampa, FL.

(37) Brookes, E., Cao, W., and Demeler, B. (2010) A two-dimensional spectrum analysis for sedimentation velocity experiments of mixtures with heterogeneity in molecular weight and shape. *Eur. Biophys. J. 39*, 405–414.

(38) Demeler, B., and van Holde, K. E. (2004) Sedimentation velocity analysis of highly heterogeneous systems. *Anal. Biochem. 335*, 279–288.

(39) Brookes, E., and Demeler, B. (2006) Genetic Algorithm Optimization for Obtaining Accurate Molecular Weight Distributions from Sedimentation Velocity Experiments. In *Analytical Ultracentrifugation VIII* (Wandrey, C., and Cölfen, H., Eds.) pp 33−40, Springer, Berlin.

(40) Brookes, E. H., and Demeler, B. (2007) Parsimonious regularization using genetic algorithms applied to the analysis of analytical ultracentrifugation experiments. In *Proceedings of the 9th annual conference on genetic and evolutionary computation*, pp 361−368, ACM, London.

(41) Demeler, B., and Brookes, E. (2008) Monte Carlo analysis of sedimentation experiments. *Colloid Polym. Sci. 286*, 129–137.

(42) Demeler, B., Brookes, E., Wang, R., Schirf, V., and Kim, C. A. (2010) Characterization of reversible associations by sedimentation velocity with UltraScan. *Macromol. Biosci. 10*, 775–782.

(43) Cao, W., and Demeler, B. (2008) Modeling analytical ultracentrifugation experiments with an adaptive space-time finite element solution for multicomponent reacting systems. *Biophys. J. 95*, 54–65.

(44) Jin, L. W., Ninomiya, H., Roch, J. M., Schubert, D., Masliah, E., Otero, D. A., and Saitoh, T. (1994) Peptides containing the RERMS sequence of amyloid β/A4 protein precursor bind cell surface and promote neurite extension. *J. Neurosci. 14*, 5461–5470.

(45) Popp, G. M., Graebert, K. S., Pietrzik, C. U., Rosentreter, S. M., Lemansky, P., and Herzog, V. (1996) Growth regulation of rat thyrocytes (FRTL-5 cells) by the secreted ectodomain of β-amyloid precursor-like proteins. *Endocrinology 137*, 1975–1983.

(46) Beher, D., Hesse, L., Masters, C. L., and Multhaup, G. (1996) Regulation of amyloid protein precursor (APP) binding to collagen and mapping of the binding sites on APP and collagen type I. *J. Biol. Chem. 271*, 1613–1620.

(47) Mok, S. S., Sberna, G., Heffernan, D., Cappai, R., Galatis, D., Clarris, H. J., Sawyer, W. H., Beyreuther, K., Masters, C. L., and Small, D. H. (1997) Expression and analysis of heparin-binding regions of the amyloid precursor protein of Alzheimer's disease. *FEBS Lett. 415*, 303–307.

(48) Kraulis, P. (1991) MOLSCRIPT: A program to produce both detailed and schematic plots of protein structures. *J. Appl. Crystallogr. 24*, 946–950.